Mixing of Fluids Flowing Through Beds of Packed Solids

EARL A. EBACH and ROBERT R. WHITE

University of Michigan, Ann Arbor, Michigan

While there have been numerous investigations of radial mass and heat transport in packed beds (*3, 7, 12, 15, 20*), axial mixing in the direction of flow has been neglected until recently because of experimental and analytical difficulties. Lapidus and Amundson (*11*) presented a mathematical treatment for adsorption in beds, including axial mixing, which involved the response function of the system to an inlet step function change in concentration. Danckwerts (*4*) arrived at similar results and determined an axial mixing factor for water flowing through packed Raschig rings at a single Reynolds number. Employing a frequency response technique, Kramers and Alberda (*10*) presented two experimental results for axial diffusion in a system similar to that of Danckwerts'. More recently, McHenry and Wilhelm (*14*) employed this method of sinusoidally varying concentrations in the study of axial mixing of binary gas mixtures flowing through a random bed of spheres. Additional mathematical analyses for the longitudinal mixing of fluids in flow through reactors have been presented by Levenspiel and Smith (*13*), Klinkenberg and Sjenitzer (*9*), Wehner and Wilhelm (*19*) and Aris and Amundson (*1*).

Previous investigations have thus resulted in data concerning the radial mixing of both gases and liquids flowing through fixed beds, and the axial mixing of gases flowing through fixed beds of spheres. The data of Kramers and Alberda, and of Danckwerts were all that existed for axial mixing in liquid systems. This study was undertaken to extend the limited data and to investigate more thoroughly the axial mixing of liquids flowing through fixed beds of solids. The variables which were investigated were fluid velocity, particle diameter, particle shape, and liquid viscosity.

EXPERIMENTAL

Methods

Four different techniques have been employed in the investigations of mixing in fixed beds. Each method analyzes the response curve resulting from some kind of initial disturbance in a dynamic system. In the *point source* method the initial disturbance is the diffusion of a tracer from a point source into the flowing fluid (*3, 7, 12, 15*). For *frequency response* experiments, the inlet concentration is varied as a harmonic function of time (*5, 10, 14*). In the *step-function* method an instantaneous change in tracer concentration occurs at the inlet (*4, 11*). The initial disturbance in the *pulse-function* method is the instantaneous injection of a concentrated tracer into the flowing liquid (*4, 22*).

Two techniques were employed in the present research.

The first approach, the *frequency-response technique*, required the response to a sinusoidally varying inlet concentration. By comparing the amplitudes of the inlet and outlet waves, the axial mixing coefficient can be determined. The frequency response method was employed in part of the present research because it presented advantages of simplicity during both the experimental work and calculations. However, analytical difficulties were encountered in the low flow-rate range because of the length of the runs and the small axial mixing rates.

The second method used, the *pulse-function* method, was employed by Yagi and Miyauchi (*22*) in their study of mixing in continuous flow reactors. Danckwerts (*4*) suggested this method for the investigation of mixing in packed beds. In this method, one determines the exit concentration profile for an experiment in which the tracer is injected over a short period of time, that is, in the form of a unit pulse. From the exit concentration profile, the axial mixing coefficient can be calculated. The pulse function technique was used during the present research for the low flow-rate range.

Flow Systems

The flow system for the frequency response experiments is shown in Figure 1. The liquid solutions were forced under constant pressure through the system from feed tanks containing a clear solution and a dye solution. The clear and dye solutions were alternated by the three-way directional-flow solenoid valve and partially mixed during flow through the pre-bed, thus forming a periodically varying concentration wave. The liquids then flowed through the packed test section, the calming section, and flowmeters. Analyses of the flowing streams were made at both the inlet and outlet of the testing section by means of continuous photometers.

The pre-bed served two purposes: first it produced an approximate constant velocity profile at the inlet testing section. Studies by Schwartz and Smith (*17*), by Thatcher (*18*) and by Hirai (*8*) indicated that for a ratio of particle diameter to tube diameter less than 0.04 the assumption of uniform velocity distribution for fluids in packed beds is valid. The pre-beds used in the experiments met this condition. The second purpose of the pre-bed was to disperse or mix the interfaces of the alternate solutions so that an approximate sine wave composition would be obtained. The pre-bed, through the mixing process, served as a damping factor, which removed most of the higher harmonics from the approximate square waves which were introduced by the three-way valve.

Essentially the same flow system was employed for the pulse-function runs except for minor modifications. A small cylinder containing the concentrated tracer solution replaced one of the larger storage tanks. The clear liquid flowed continuously through the system. A short dye pulse was injected into the flowing stream by means of the three-way directional-flow solenoid valve. The pre-bed was not used; hence longer test columns were employed. The liquid flowing through the column was analyzed only at the outlet of the testing section by a continuous photometer.

Test Column

Figure 2 is a sectional drawing of the column showing the several sections flanged together in preparation for a frequency response run. Two ¾-in. glass spacers used in the analytical system separated the test section from the pre-bed and the calming section. All glass sections of the column were 2-in. I.D. Pyrex glass pipe. The spacers, gaskets, and brass calming section were likewise 2-in. I.D. so as to maintain a smooth wall across the joints. Two-, three- and five-foot lengths were used for the test sections.

Glass spheres, Raschig rings, Berl saddles, and Intalox saddles were used as packing. The characteristics of the packings are shown in Table 1. The porcelain packings were supplied through the courtesy of the United States Stoneware Company. The void space in the packed beds was determined by measuring the volume of water in a length of the unpacked column and in the same length of a packed column. The same method of packing, i.e., pouring a small amount of beads and tapping the column to promote settling, was used each time the column was repacked. The packing was supported on a 100-mesh screen.

Analytical System

Pontamine Sky Blue 6BX dye was employed as the tracer. The concentration profiles were measured as a function of time by continuous colorimetric photometers which gave an instantaneous measurement of the fluid composition flowing through a

E. A. Ebach is presently with the Dow Chemical Company, Midland, Michigan.

TABLE 1.—PACKING CHARACTERISTICS

Type	Material	Nominal Size	Equivalent Diameter d_p	d_p/d_t	Bed Porosity ϵ
Spherical	Glass	60/80 mesh	.0083 in.	.0042	.352
Spherical	Glass	1 mm	.039 in.	.020	.340
Spherical	Glass	3 mm	.133 in.	.067	.340
Spherical	Glass	6 mm	.265 in.	.13	.367
Raschig rings	Porcelain	1/4 in.	.22 in.	.11	.632
Berl saddles	Porcelain	1/4 in.	.23 in.	.12	.616
Intalox saddles	Porcelain	1/4 in.	.20 in.	.10	.629

horizontal section of the column. The thin light beams passed through the glass spacers on a diameter just above or just below the test section. Details of the design and construction of the photoelectric colorimeters are available elsewhere (*6*). The output of the phototube circuit was measured by a Leeds and Northrup Speedomax Indicating Recorder.

Most runs were made with dilute water solutions. A few runs employed mixtures of propylene glycol and water to vary the viscosities of the liquid. All runs were made with a completely flooded column.

Experimental Procedure and Data

For each frequency-response run a pre-bed, having a suitable height and particle diameter to produce a satisfactory periodic wave in the desired frequency and flow rate, was installed above the test column. Dynamic calibrations of the inlet and outlet colorimeters were made, first with the clear and then with the dye solution. The timer, set at a predetermined frequency and controlling the three-way directional-flow solenoid valve, was started. Recorder traces were then obtained for both the inlet and outlet wave concentrations.

Typical *experimental data* (*6*) for the *frequency-response runs* are presented in Table 2. The corrected interstitial velocity of the liquid solutions is reported in column 2. The maximum and minimum concentration points, averaged for ten inlet periodic waves, are presented in columns 3 and 4, respectively; the maximum and minimum concentration, averaged for the ten corresponding outlet waves is presented in columns 6 and 7, respectively. Typical curves are shown in Figure 3, which presents the inlet and outlet waves for Run 28 resulting after the conversion to concentration units. The points are averages of experimental concentrations, while the lines are true sinusoidal waves.

The experimental procedure for the pulse function method was as follows: the flow rate and temperature of the clear solution was adjusted as desired. The outlet colorimeter was calibrated with the clear flowing liquid. A stopwatch was employed to measure the residence time of the injected concentrated dye. A recorder trace was then obtained for the outlet pulse wave. This procedure was repeated several times for a given flow rate.

Typical *experimental data* for the *pulse-function* runs are presented in Table 3. Column 2 contains the corrected liquid interstitial velocity. The data for an exit pulse profile, averaged from the recorder traces of three or more waves, are presented in columns 3 and 4. Column 3 contains the maximum value of the pulse wave in concentration units and column 4 the area under the exit concentration profile of the pulse wave.

TREATMENT OF EXPERIMENTAL DATA

As a fluid, in which concentration gradients exist, flows through a packed bed, eddy diffusion or mixing occurs which can be described by the equation

$$N = -(D_v + \delta_E)\frac{dc}{dy} = -D_T\frac{dc}{dy} \quad (1)$$

A material balance for an increment of time dt made for a cylindrical element dr in thickness and dz in height results in the equation:

$$D_R\left[\frac{\partial^2 c}{\partial r^2} + \frac{1}{r}\frac{\partial c}{\partial r}\right] + D_L\frac{\partial^2 c}{\partial z^2} - u\frac{\partial c}{\partial z} = \frac{\partial c}{\partial t} \quad (2)$$

In theory, determinations of concentration, c, as a function of position, r and z, and time, t, in an experiment where a tracer is fed at a point source into fluid of known composition and flow rate, yield the information required to determine D_R and D_L through the evaluation of the various first and second partial derivatives by numerical differentiation and smoothing. The difficulties of obtaining such data and the large error involved in differentiating the data twice, lead to special experimental conditions for which Equation (2) has known mathematical solutions which permit the evaluation of effective diffusivity from specific values of c, r, z, and t. The point-source experiment results in the evaluation of effective radial diffusivity, D_R, while other types of experiments lead to values of effective axial diffusivity, D_L.

Frequency-Response Experiment

In the frequency-response method the concentration at the inlet is varied sinusoidally and the response is obtained at the outlet. Comparison of the amplitudes of the inlet and outlet harmonic functions leads to values of the axial diffusivities.

Mathematical Representation

Sinusoidal Solutions. In the mathematical representation of the frequency-response experiment, no radial concentration gradients exist and the effective axial diffusivity and velocity are independent of position leading to the modification of Equation (2) as follows:

$$D_L\frac{\partial^2 c}{\partial z^2} - u\frac{\partial c}{\partial z} = \frac{\partial c}{\partial t} \quad (3)$$

The two experimental boundary conditions which were chosen are: first, the inlet concentration is a harmonic function of time; second, at a sufficiently long distance down the bed the amplitude approaches zero. These boundary conditions can be represented as follows:

$$c(0, t) = c_m + A(0)\cos\omega t \quad (3a)$$
$$c(\infty, t) = c_m \text{ or } A(z) = 0 \text{ for } z \to \infty$$

With the introduction of the above boundary conditions, the periodic steady-state solution resulting is:

$$c(z, t) = c_m + A(0)e^{-B}\cos(\omega t - \phi) \quad (4)$$

where

$$B = -\frac{zu}{2D_L}\cdot\left\{1 - \sqrt{\sqrt{\frac{1}{4} + \left(\frac{2D_L\omega}{u^2}\right)^2} + \frac{1}{2}}\right\} \quad (4a)$$

and

$$\phi = \frac{zu}{2D_L}\sqrt{\sqrt{\frac{1}{4} + \left(\frac{2D_L\omega}{u^2}\right)^2} - \frac{1}{2}} \quad (4b)$$

The functions B and ϕ are representative of the decrease in amplitude and the

TABLE 2.—TYPICAL EXPERIMENTAL DATA AND CALCULATED RESULTS * FREQUENCY RESPONSE TECHNIQUE

1	2	3	4	5	6	7	8	9	10	11	12
					Periodic wave data						
Run	Interstitial velocity ft./sec.	Inlet wave Maximum concentration	Inlet wave Minimum concentration	Inlet wave Amplitude A_i	Outlet wave Maximum concentration	Outlet wave Minimum concentration	Outlet wave Amplitude A_e	Frequency rad./sec.	Axial diffusivity sq. ft./sec.	Reynolds number $d_p v_0$	Peclet number $\frac{d_p u}{D_L}$
					Particle diameter 0.039 in.; porosity 0.34; height 3.01 ft.						
8	0150	.757	.244	.513	.633	.367	.266	.0785	.000119	1.60	.41
7	.0151	.789	.212	.577	.726	.273	.453	.0519	.000103	1.61	.52
6	.0224	.808	.192	.616	.734	.267	.467	.0850	.000144	2.35	.50
9	.0224	.734	.267	.467	.634	.367	.267	.126	.000132	2.58	.55
5	.0326	.853	.147	.706	.751	.250	.501	.126	.000254	3.65	.38
4	.0788	.861	.138	.723	.749	.250	.499	.313	.000617	8.21	.43
3	.146	.881	.120	.761	.781	.220	.561	.523	.00116	15.35	.39
2	.210	.868	.132	.735	.766	.235	.531	.785	.00164	22.16	.41
1	.270	.918	.082	.836	.840	.160	.680	.785	.00233	29.54	.36
					Particle diameter 0.0083 in.; porosity 0.35; height 3.04 ft.						
25	.00647	.856	.144	.712	.807	.193	.614	.0419	.0000075	.15	.60
26	.0122	.830	.171	.659	.776	.224	.552	.0785	.0000175	.28	.48
21	.0193	.876	.124	.752	.825	.175	.650	.105	.0000316	.42	.42
22	.0293	.876	.124	.752	.820	.180	.640	.157	.0000543	.63	.37
23	.0630	.887	.113	.774	.835	.166	.669	.314	.000121	1.38	.36
20	.0658	.752	.247	.505	.724	.275	.449	.314	.000164	1.64	.30
24	.101	.913	.087	.826	.873	.125	.748	.449	.000168	1.68	.41
19	.190	.797	.203	.594	.772	.228	.544	.785	.000468	5.06	.30

phase shift of the outlet wave, respectively.

Boundary conditions, other than that employed above, have been reported (*4, 10*), which eventually lead to the same approximate solution as Equation (5) below. The space required for analysis during these experiments was held to a minimum, thus maintaining bed continuity across the boundaries. Hence the above infinite column boundary conditions, Equation (3*a*), appear compatible with the experimental technique employed.

Approximate Solution. An approximate form of the above solution can be employed when experimental conditions are such that the ratio, $4\omega D_L/u^2$, is small. By changing Equation (4) to complex form, expanding the radical by means of the Binomial Theorem and rejecting the imaginary terms, the following approximate solution is obtained:

$$c(Z, t) = c_m + A(0) \cdot \exp\left\{\left(-\frac{Z\omega^2 D_L}{u^3} + \frac{5Z\omega^4 D_L^3}{u^7} \cdots\right)\right\} \cdot \cos\left(\omega t \frac{Z\omega}{u} + \frac{2Z\omega^3 D_L^2}{u^5} \cdots\right) \quad (5)$$

The value of B can be approximated, assuming the terms beginning with $5z\omega^+D_L^3/u^7$ are insignificant, as

$$B \cong \frac{z\omega^2 D_L}{u^3} \quad (5a)$$

The ratio of inlet to outlet amplitudes then leads to the equation

$$\ln \frac{A_i}{A_e} = B \cong \frac{z\omega^2 D_L}{u^3} \quad (5b)$$

from which D_L can be calculated. For experiments in which the term, $5z\omega^4 D_L^3/u^7$, is significant, the ratio of amplitudes can be approximated by the equation

$$\ln \frac{A_i}{A_e} = B \cong \frac{z\omega^2 D_L}{u^3} - \frac{5z\omega^4 D_L^3}{u^7} \quad (6)$$

from which D_L can be calculated by trial and error. The diffusivities were calculated by one of the above approximations so that the maximum error in the value of B caused by the approximation is less than 1.5%, which is well within the error of measurement.

Evaluation of axial diffusivity from

TABLE 3.—TYPICAL EXPERIMENTAL DATA AND CALCULATED RESULTS * PULSE FUNCTION TECHNIQUE

1	2	3	4	5	6	7	8	9
Run	Interstitial velocity u	Average pulse data Maximum Concentration	Average pulse data Area Under Pulse Profile	Maximum concentration of pulse $\left(\frac{Vc}{Q}\right)_{R=\gamma}$	Residence time of pulse	Axial Diffusivity	Reynolds number	Peclet number
	ft./sec.	g./liter × 10^2	g./liter × 10^2		R	sq. ft./sec.	$\frac{d_p v_{0\rho}}{\mu}$	$\frac{d_p u}{D_L}$
				60/80 Mesh spheres—particle diameter 0.0083 in.; porosity 0.35; height 5.12 ft.				
P15	.000773	.391	.0305	12.81	1.35	.00000105	.021	.51
P16	.00154	.539	.0407	13.24	1.16	.00000265	.040	.40
P17	.00232	.400	.0254	15.86	1.13	.00000294	.062	.54
P18	.00310	.543	.0362	14.98	1.08	.00000486	.085	.44
P19	.00587	.439	.0262	16.72	1.09	.00000727	.16	.56
P20	.00879	.562	.0327	17.19	1.05	.0000111	.23	.55
P21	.0145	.632	.0347	18.23	1.04	.0000164	.38	.61
P22	.0215	.428	.0231	18.54	1.03	.0000239	.56	.62
P23	.0315	.557	.0318	17.51	1.02	.0000402	.82	.54
				¼ in. Raschig rings—particle diameter 0.27 in.; porosity 0.62; height 5.0 ft.				
P32	.00333	.455	.169	2.69	1.04	.000169	3.81	.36
P30	.00811	.569	.201	2.83	1.00	.000405	9.28	.37
P31	.0174	.589	.203	2.91	1.00	.000830	20.4	.39
P29	.0362	.372	.117	3.17	1.01	.00140	40.4	.47

measurement of the phase angles was not carried out during the present research, since the measurements of amplitude ratios provided a more accurate and reliable means of evaluation. Axial diffusivities calculated from phase shift gave poor accuracy and reproducibility.

Nonsinusoidal Solution. The outlet wave from the pre-bed, or the inlet wave to the test section, was not always sinusoidal although periodic. Under these conditions, the periodic concentration wave could be represented by a Fourier series having the form

$$c(0, t) = \frac{a_0}{2} + \sum_{n=1}^{\infty} (a_n \cos n\omega t + b_n \sin n\omega t) \quad (7)$$

or the form

$$c(0, t) = \frac{a_0}{2} + \sum_{n=1}^{\infty} (A_n(0) \cos (n\omega t - \psi_n) \quad (7a)$$

where

$$A_n(0) = [a_n^2 + b_n^2]^{\frac{1}{2}}$$

represents the amplitude of the n-th harmonic and

$$\psi_n = \tan^{-1} \frac{b_n}{a_n} \quad (7c)$$

represents the phase lag of the n-th harmonic with reference to a pure cosine wave of the same frequency. Thus, as the above equations indicate, the periodic function is a combination of simple harmonic waves. The term $a_0/2$ represents the neutral position: the terms, $a_1 \cos \omega t + b_1 \sin \omega t$, the fundamental wave; and the other terms, $a_n \cos n\omega t + b_n \sin n\omega t$, the higher harmonics. The outlet concentration wave then also must be represented by a Fourier series in which each harmonic component is damped and shifted in phase. By the principle of superposition, each harmonic in the outlet corresponds to the outlet expected if the corresponding harmonic in the inlet wave was the only inlet. Applying the periodic, but non-sinusoidal, inlet wave as a boundary value to the differential equation for the diffusion-convection mixing of a liquid flowing through fixed beds, results in the approximate solution

$$c(z, t) = \frac{a_0}{2} \cdot \sum_{n=1}^{\infty} A_n(0) \exp\left\{-\left[\frac{zn^2\omega^2 D_1}{u^3}\right]\right\} \cdot \cos\left(n\omega t - \psi_n - \frac{nz\omega}{u}\right) \quad (8)$$

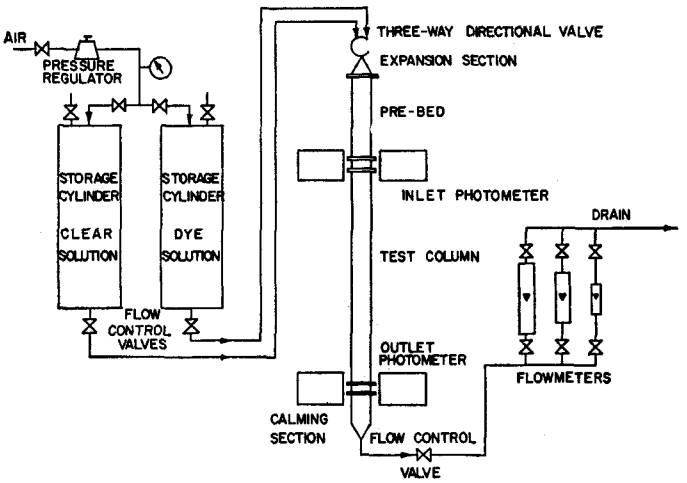

Fig. 1. Flow-system-frequency-response experiments.

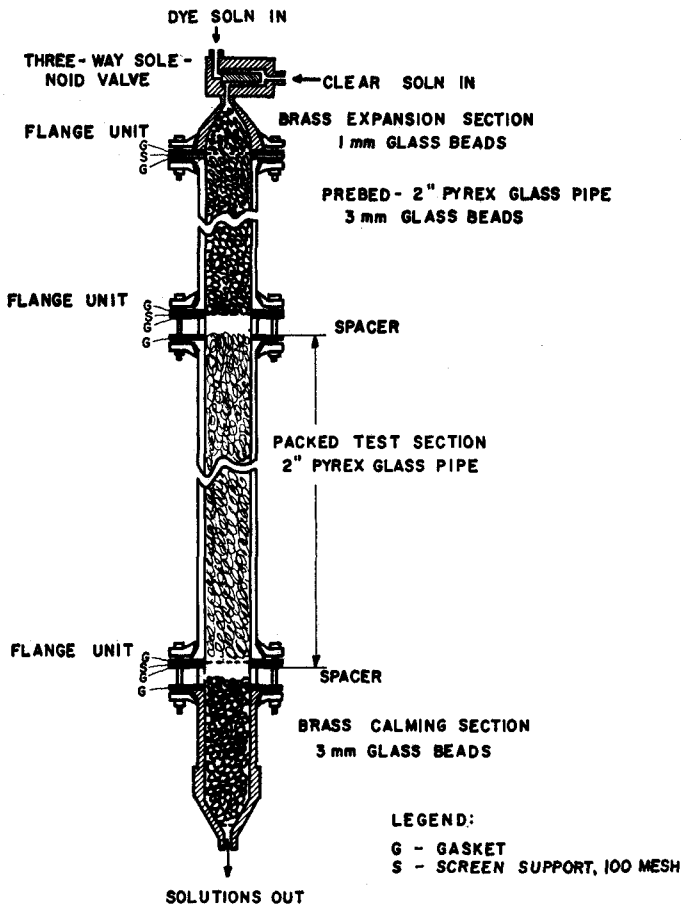

Fig. 2. Column-detail-frequency-response technique.

This solution confirms the earlier statement that each harmonic component is dampened and shifted in phase. The fact that a periodic function can be resolved into its simple harmonic components permits the reduction of the inlet wave to its simple harmonic components, the application of each component to the system, and the construction of the general outlet case by addition of the components. The application of the frequency response method to the periodic concentration waves requires a harmonic analysis of the experimental functions, that is, a representation of the functions as Fourier Series.

Sinusoidal Data. For the sinusoidal input concentration waves, the ratio of the inlet and outlet amplitudes was used to calculate the longitudinal diffusivity according to Equation (5*b*) or (6).

The amplitude ratio was determined

in the following manner: the minimum and maximum concentrations for ten consecutive inlet sinusoidal waves and their corresponding outlet waves were averaged and were reported as in columns 3, 4, 6, and 7, respectively, of Table 2. From these concentrations the amplitudes (columns 5 and 8), and hence the amplitude ratio, A_i/A_e, lead to the calculation of the axial diffusivity, D_L, (column 10) as described above.

Nonsinusoidal Data. For nonsinusoidal input waves the experimental inlet composition wave must be converted into a form of the Fourier series. A numerical procedure known as the 12-ordinate scheme of harmonic analysis, discussed in Wylie (*21*), was used to determine the coefficients in the Fourier series. This numerical procedure is equivalent to the graphical method of approximating the periodic concentration wave when a series of harmonics, whose sum approaches that of the given periodic function is assumed. For the numerical harmonic analysis the values of the concentration wave at intervals of one twelfth of a period were obtained by averaging a series of ten periodic inlet waves. From these concentration values, $c_0, c_1, \ldots c_{12}$, the values of the Fourier coefficients a_n and b_n were obtained by a series of successive condensations. The Fourier series for the inlet wave resulting from the numerical analysis has the form:

$$c(0, t) = \frac{a_0}{2} + a_1 \cos \omega t + b_1 \sin \omega t \cdots + a_5 \cos 5\omega t + b_5 \sin 5\omega t \quad (8)$$

The corresponding series for the outlet wave must be

$$c(z, t) = \frac{a_0}{2} + a_1 e^{-B} \cos \delta + b_1 e^{-B} \sin \delta \cdots + a_n e^{-n^2 B} \cos n\delta + b_n e^{-n^2 B} \sin n\delta \cdots + a_5 e^{-25B} \cos 5\delta + b_5 e^{-25B} \sin 5\delta \quad (9)$$

where

$$\delta = \omega t - \phi$$

The equation for B, approximated by the methods previously presented for sinusoidal waves, is:

$$B \cong \frac{z\omega^2 D_L}{u^3} \quad (5a)$$

The maximum concentration, $c(z, t)_{max}$, and the corresponding angle, δ, were averaged for the ten outlet waves. Substitution of these values, $c(z, t)_{max}$ and δ, and the coefficients a_n and b_n, determined from the harmonic analysis of the inlet wave, into Equation (9), results, after a trial-and-error procedure in a value of B based upon the maximum concentration of the outlet wave. The calculation of B was simplified because the third and higher terms of the series represented by Equation (9) were small, and the exponential approached zero rapidly. This value of B for the peak concentration was then used to compute the entire outlet wave according to Equation (9). Comparison of the calculated wave with the experimental outlet wave indicated that the evaluation of B from Equation (9), by substituting the value of the peak and angle of the outlet concentration wave, was valid. In Figure 4, the upper wave is the inlet nonsinusoidal wave employed to evaluate the coefficients of the Fourier series. The lower curve is the experimental outlet wave, and the points are those calculated from Equation (9) with values of B determined from the maximum outlet concentration point. The axial diffusivity was then determined from Equation (5*a*).

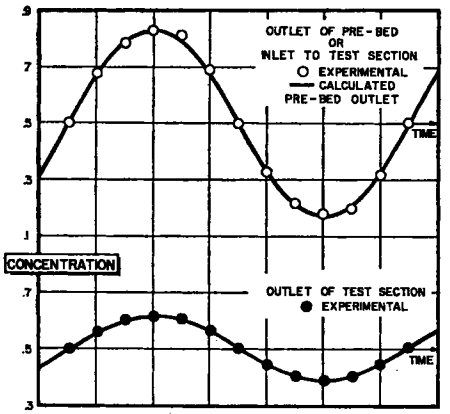

Fig. 3. Periodic sinusoidal waves (run 28). Prebed: 3-mm. spheres, height 1.5 ft.

Pulse-Function Experiment

It should also be possible to evaluate the axial mixing of liquids flowing through fixed beds from the shape of an outlet concentration profile resulting from a step function change in concentration at the inlet (*4, 11, 19*). However, experimental difficulties were encountered in obtaining a true step function and failure of this method to give reproducible results led to the consideration and use of the pulse function method (*4, 13*).

Mathematical Representation. The pulse-function method is an extension of the step-function approach. The inlet boundary conditions are obtained by injecting instantaneously into the flowing stream a concentrated tracer solution. The concentration profile for the pulse is determined at the outlet of the test section. Danckwerts (*4*) has shown that the exit concentration profile for a unit pulse is the derivative of the dissribution function for a step function. Step-function experiments had indicated that adsorption of the tracer substance occurred at low flow rates. Since the pulse-function runs were made at low flow rates, adsorption of the tracer also occurred. The mathematics of longitudinal diffusion combined with adsorption for fluids flowing through packed beds have been discussed by Lapidus and Amundson (*11*). The diffusion convection Equation (3), modified to include the adsorption effect, is

$$D_L \frac{\partial^2 c}{\partial z^2} - u \frac{\partial c}{\partial z} = \frac{\partial c}{\partial t} + \frac{1}{\epsilon} \frac{\partial \eta}{\partial t} \quad (10)$$

where

η = amount of tracer adsorbed on the particle surface

ϵ = fractional void volume in the bed.

The solution to Equation (10) with the boundary conditions for an inlet step function for a finite column

$$\left.\begin{aligned} c(z, 0) &= 0 \quad z < 0 \\ \eta(z, 0) &= 0 \quad z > 0 \end{aligned}\right\} \quad (10a)$$

$$c(0, t) = 1 \quad t > 0 \quad (10b)$$

and an assumed adsorption mechanism

$$\eta = k_1 c + k_2 \quad (10c)$$

is

$$\frac{c}{co} = \frac{1}{2}\left\{1 + erf\left(\frac{R - \gamma}{\sqrt{4R\gamma S}}\right) + e^{1/S} erfc\left(\frac{R + \gamma}{\sqrt{4R\gamma S}}\right)\right\} \quad (11)$$

where

$\gamma = 1 + \frac{k_1}{\epsilon}$, dimensionless adsorption factor

$R = \frac{ut}{z}$, dimensionless time variable

$S = \frac{D_L}{zu}$, dimensionless mixing factor

The formula for the concentration profile for the unit pulse, resulting from the differentiation of Equation (11), is

$$\frac{V_c}{Q} = \frac{1}{4\pi}\left\{\frac{R + \gamma}{\sqrt{R^3 S\gamma}} \cdot \exp\left\{-\left(\frac{R - \gamma}{\sqrt{4RS\gamma}}\right)^2\right\} - \frac{R - \gamma}{\sqrt{R^3 S\gamma}} \cdot \exp\left\{\frac{1}{S} - \left(\frac{R + \gamma}{\sqrt{4RS\gamma}}\right)^2\right\}\right\} \quad (12)$$

where Q is the quantity of tracer injected into the feed stream at time 0 and V is the void volume of the bed. Similar results have been obtained by Levenspiel and Smith (*13*). The values of S and γ can be determined so that a calculated distribution curve will approximately

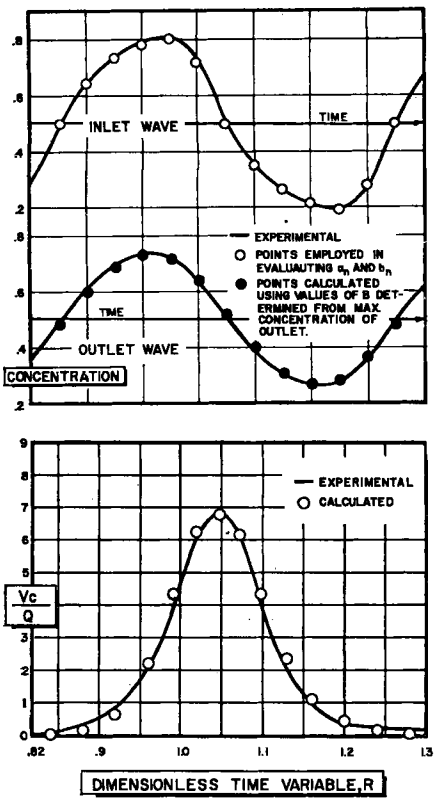

Fig. 5. Comparison of experimental and calculated outlet pulse function waves.

Fig. 4. Variation of axial diffusivity with viscosity at constant velocity ($u \cong 0.0023$ ft./sec.) and constant particle diameter ($d_p = 0.039$ in.).

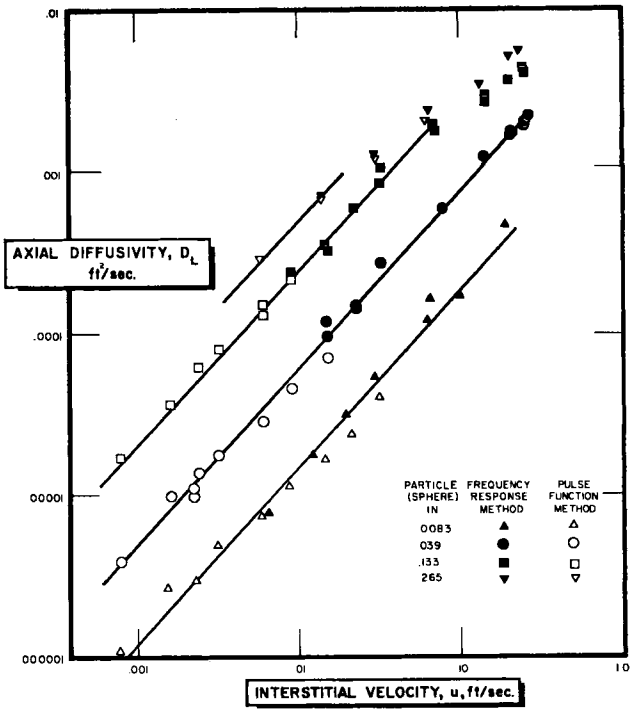

Fig. 6. Dependency of axial diffusivity on particle diameter, plot of $C_1 = Cd_p^a$ where $D_L = Dd_p^a u^b = C_1 u^b$.

duplicate an experimental concentration profile. The adsorption mechanism, Equation (10c), which indicates that equilibrium is established at each point in the bed, was assumed for mathematical convenience and when checked against experimental pulse waves appeared to be a satisfactory mechanism.

Evaluation of Data: During this research the pulse-function method was employed for runs made at low liquid flow rates, and also for runs using nonspherical particles. The fact that the area under the concentration profile for a unit pulse is equal to unity was of value in evaluating the axial diffusivity. The exit concentration profiles recorded on the chart paper were converted to the proper concentration units and time units; i.e, Vc/Q and R (columns 5 and 6, respectively, Table 3). After several trial-and-error calculations on a series of runs in which S and γ were approximated in order to duplicate an experimental pulse wave, it was found that under the experimental conditions used, the peak of the concentration profile occurred at $R = \gamma$. Hence, the value of Vc/Q at the peak, determined by setting $\gamma = R$ in Equation (12), is

$$\left(\frac{V_c}{Q}\right)_{R=\gamma} = \frac{1}{2R\sqrt{\pi S}} = \sqrt{\frac{zu}{4\pi R^2 D_L}} \qquad (13)$$

from which D_L can be calculated. The feasibility of using the maximum point on the pulse function to calculate the axial diffusivity is shown in Figure 5, which is typical of the pulse-function runs. The curve is the experimental pulse profile, and the points are calculated from Equation (12) with the use of an axial diffusivity determined from the peak point.

A differentiation of Equation (12) to determine the time at which the maximum occurs in the output pulse does not indicate that $R = \gamma$, and thus there is an inconsistency between the experimental data and Equation (12). However, the experimental value of R was always close to unity and the inconsistency was small as indicated by the agreement between the experimental data and the calculated curve in Figure 5.

RESULTS

The prime variables affecting axial mixing which were investigated were liquid velocity, particle size, particle shape and liquid viscosity.

Liquid Velocity and Particle Size

A series of experiments was made with spheres for each of four particle sizes (0.0083, 0.039, 0.133 and 0.265 in.) in which the interstitial velocity was varied from 0.0008 to 0.3 ft./sec. A plot of the logarithm of axial diffusivity as a function of the logarithm of interstitial velocity with particle size as parameter is presented in Figure 6. Data from the two experimental techniques, the frequency response method (solid symbols) covering the high flow rates and the pulse-function method (empty symbols) covering the low flow rates, are presented in the figure. The data from both techniques for a single particle size results in a straight-line relationship between the logarithm of axial diffusivity and the logarithm of interstitial velocity. The correlation of data obtained by both methods indicated the axial diffusivity measurements were quite reliable and not dependent upon the experimental technique employed.

The family of straight lines in Figure 6 is drawn with equal slopes. The separate slopes of each set of data were obtained by least squares, and the common slope was determined by a simultaneous least-squares method. Statistical tests indicate that the differences between the individual slopes and the common slope might reasonably be caused by sampling variation, i.e., the common slope does not differ significantly from the individual slopes (*16*). The value of the common slope is 1.08 and its standard deviation is ± 0.02. Statistical tests also indicate that a common theoretical slope of one, which would result if the axial diffusivity were directly proportional to the interstitial velocity, differs significantly from the slopes obtained from the experimental data.

In Figure 6 the straight-line relationship does not exist for the 0.133-in. spherical particles for interstitial velocities greater than 0.06 ft./sec. In this range the axial diffusivity does not increase as rapidly with the increase in interstitial velocity as in the lower range. The same is true for the 0.265-in. spheres at interstitial velocities greater than 0.02 ft./sec.

Figure 6 also indicates a relationship between axial diffusivity and particle size. The relationship between the axial diffusivity, particle size, and interstitial velocity can be represented by the equation

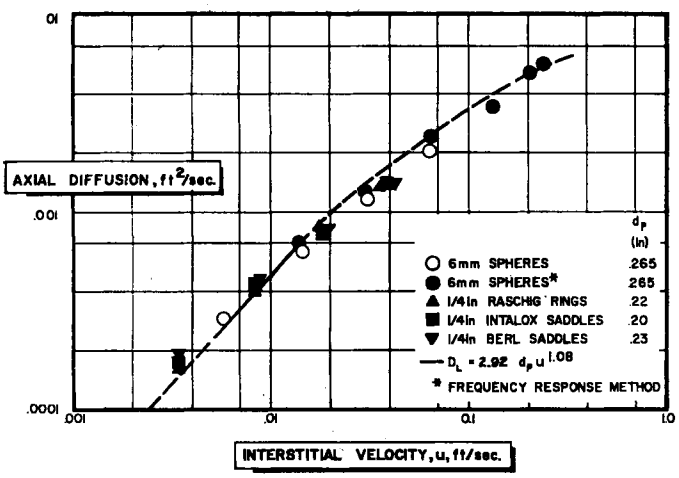

Fig. 7. Effect of particle shape.

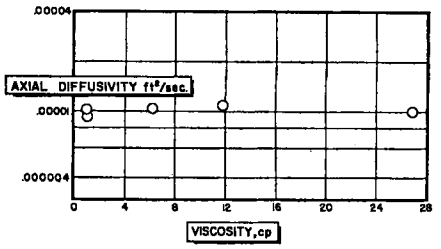

Fig. 8. Pulse function experiment, concentration profile (run P6).

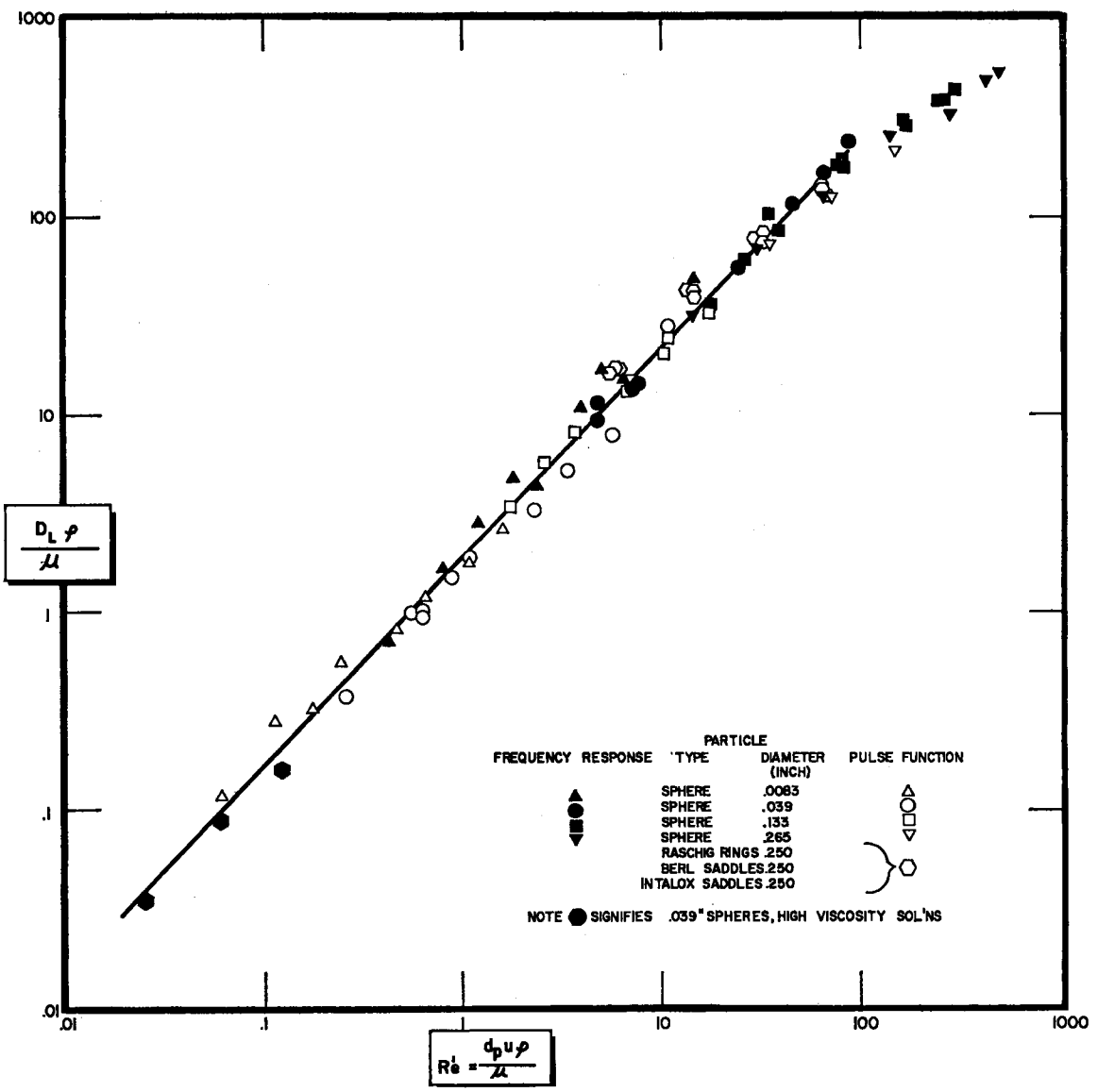

Fig. 9. Correlation of data of this investigation.

$$D_L = C\, d_p^a u^b \qquad (14)$$

The values of the coefficients, evaluated by least squares from the experimental data, are

$$D_L = 2.92\, d_p u^{1.08} \qquad (14a)$$

where

$$d_p u < 5.5 \times 10^{-4} \text{ sq. ft./sec.}$$

As indicated, this relationship is valid only in the region where the product of particle diameter and linear velocity is less than 5.5×10^{-4} sq. ft./sec., since the straight-line approximations of the experimental data exist only in this region.

Particle Shape

Several various types of packing were investigated to determine the effect of

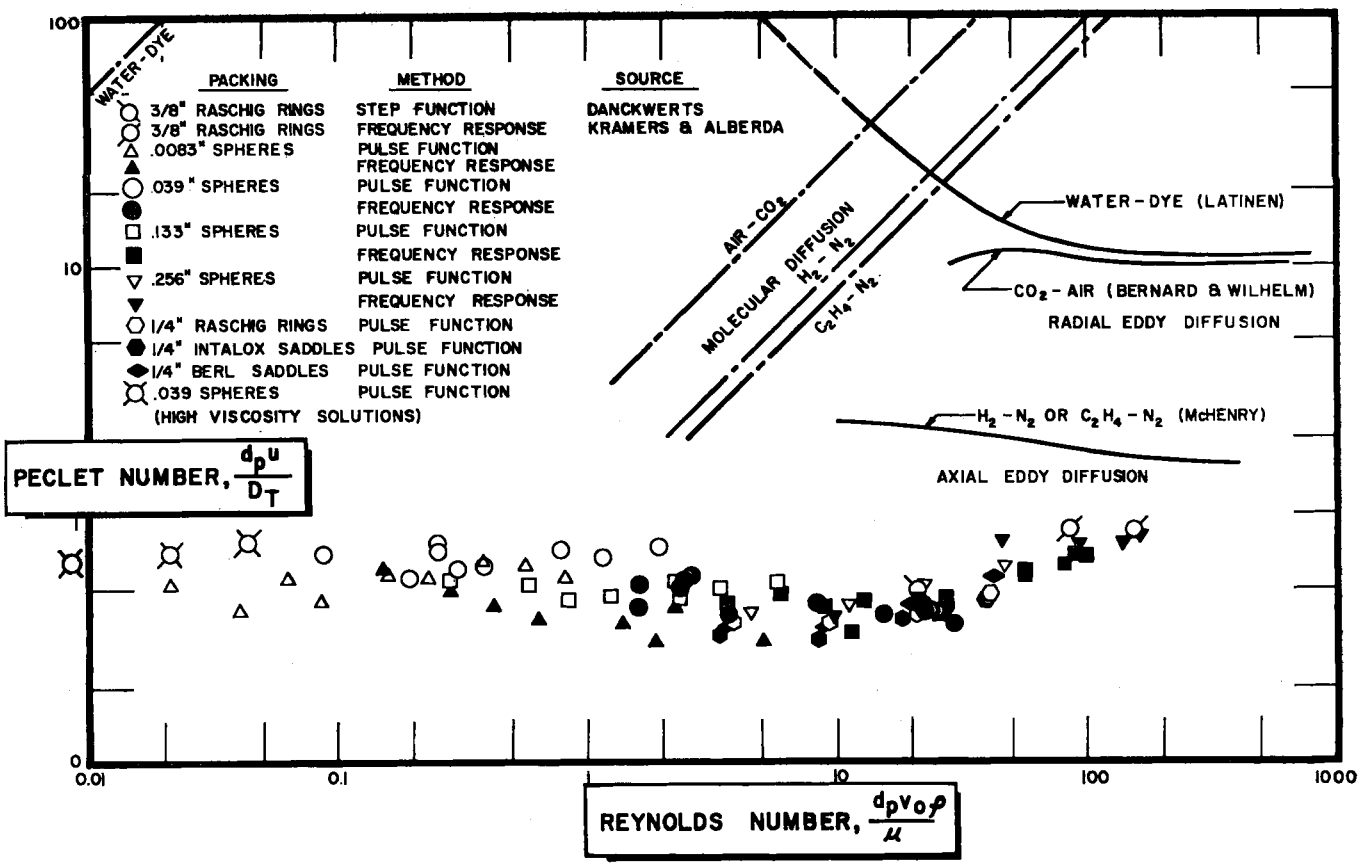

Fig. 10. Peclet number vs. Reynolds number correlation.

particle shape on the mixing of liquids flowing through a packed bed. The smallest available Raschig rings, Berl saddles, and Intalox saddles, each having a nominal size of ¼ in., were used. Glass spheres, of 6 mm. diam. were also investigated to obtain a comparison of the large odd shapes with spheres of an approximate equivalent diameter. The properties of the various packings are presented in Table 1. The data for the above packings are plotted in Figure 7 which shows the relationship between axial diffusivity and interstitial velocity. Both experimental procedures, the frequency response method, and the pulse function method, were used in obtaining data for the 6-mm. glass spheres to establish the reproducibility of the techniques for the large d_p/d_t ratio. The axial diffusivities for the other packings were obtained by pulse-function experiments. Data for all packings studied, having an equivalent diameter in the range 0.20 to 0.26 in., fall approximately along the same line. This indicates that the axial mixing is dependent upon the size of the particle and not the shape of the particle in so far as it has been investigated.

Liquid Viscosity

A series of runs was made to determine the effect of viscosity. Aqueous solutions containing various percentages of propylene glycol were used to vary the viscosity. During these experiments the particle diameter (0.039 in.) and the linear velocity (approximately 0.002 ft./sec.) were held constant, with the viscosity being the only variable. Figure 8 shows that over the viscosity range covered, 1 to 26 centipoises, there was no variation in axial diffusivity.

General Correlation

The preceding correlations suggested a relationship between the ratio, $D_L\rho/\mu$, and a modified Reynolds number, $d_pu\rho/\mu$, based upon interstitial velocity and particle diameter. The ratio, $D_L\rho/\mu$, is a dimensionless diffusivity ratio since it is actually axial diffusivity divided by kinematic viscosity. The values of $D_L\rho/\mu$ are plotted as a function of d_pu/μ in Figure 9. All the data of this investigation (86 points), even that for Raschig rings, Berl saddles, and Intalox saddles are correlated by a single curve which for values of $d_pu\rho/\mu < 100$ may be represented by the equation

$$D_L\rho/\mu = 1.92(d_pu\rho/\mu)^{1.06} \qquad (15)$$

The coefficients evaluated from the data have the following standard deviations:

$$1.92 \pm 0.02$$

$$1.06 \pm 0.01$$

In order to remove the possibility that the nonspheres were effecting the correlation, the constants were recalculated for all data obtained with spherical packing. There was no significant variation in the values of the constants.

Experimental Variables

Several variables resulting from the experimental techniques were also investigated. The frequency and amplitude of the periodic function in the frequency-response experiments were varied and found to have no effect on the axial diffusivity. A second dye was used as tracer and previous results were duplicated. The column diameter was held constant in all experiments. Several runs were made with various bed lengths and no noticeable variation in axial diffusivity measurements was observed. The length of the packed testing sections used and the method of analysis employed made end-effects negligible.

DISCUSSION

The results of this study of axial mixing in liquids flowing through beds of packed solids are graphically compared in Figure 10 with the results of other investigations concerning the axial and radial mixing of gases and liquids flowing through beds. Modified Peclet numbers, d_pu/D_L, are plotted as a function of Reynolds number, $d_pV_o\rho/\mu$. The results of this study are represented by the symbols in the lower portion of the figure. Peclet numbers varied from 0.3 to 0.8 for the range of Reynolds numbers from 0.01 to 150.

Kramers and Alberda (*10*), using the frequency-response method, investigated the longitudinal mixing of water flowing through a column (diam.: 2.9 in., length: 13.4 in.) packed with ⅜-in. Raschig rings. The value of Peclet number, 0.86, computed from the data of Kramers and Alberda, is

shown in Figure 10 for the two water velocities investigated (Reynolds numbers: 85 and 155). The data agree with the results of this research.

Another experiment concerning the axial mixing of water flowing through a bed (diam.: 1.9 in.; length: 4.6 ft.), packed with ⅜-in. Raschig rings has been presented by Danckwerts (*4*). The value of Peclet number, 0.49, for a Reynolds number of 22 is also in agreement with the data of this research as indicated by Figure 10.

Measurements on the axial mixing of binary gas mixtures flowing through a random bed of spherical particles have been reported by McHenry and Wilhelm (*14*). The test columns of 1.93 in. diam., were randomly packed with 0.127-in. spherical particles to a height varying from 1 to 3 ft. For the gas systems H_2–N_2 and C_2H_4–N_2 and for Reynolds numbers between 10 and 400, the mean of 21 determinations of axial Peclet number was 1.88 ± 0.15. The curve shown in Figure 10 summarizes graphically the data of McHenry and Wilhelm.

The axial mixing data for the gas systems does not coincide with the results for the liquid systems. The greater degree of axial mixing in liquid systems results probably from the increased by-passing, trapping, and short-circuiting of the liquid packets, since there is less efficient mixing within the void cells themselves. Thus, if the Reynolds number range were increased beyond 170 for liquid systems, the values of axial Peclet numbers would approach those of the gas system. This should result since the greater turbulence would create a higher degree of mixing in the void cells, hence less by-passing and short-circuiting, and thus less axial mixing for the bed as a whole.

A comparison of the axial mixing data with data from the literature concerning radial mixing is also made in Figure 10. The point-source method was employed to evaluate the extent of radial mixing for both liquid and gas systems. The curves shown are a summary of the data of Bernard, Latinen, and Wilhelm (*3, 12, 20*) and are representative of other radial mixing investigations (*7, 15*). The data for gas systems indicate that radial Peclet number is approximately 10 for Reynolds numbers between 25 and 600. The liquid systems show a constant Peclet number of 11 for Reynolds numbers greater than 150, with an increase in Peclet numbers below this region. The results of both investigations agree with the statistical "random-walk" approach of Baron (*2*) who predicted a Peclet number of 11 for fully developed turbulence. The above comparisons indicate that for flow through packed beds a greater degree of mixing exists in the axial direction than in the radial direction.

The curves for molecular diffusion for the three gas systems and the water-dye system are included in Figure 10. These curves indicate the large increase in mixing occurring because of processes other than molecular diffusion. At low flow rates, with other effects being negligible, the curves for effective and molecular diffusion should merge.

ACKNOWLEDGMENT

The authors express their appreciation to the Standard Oil Foundation and the Dow Chemical Company for support of graduate fellowships during the course of this work.

NOTATION

a = constant
a_n = coefficients of cosine terms of Fourier series
A_o = outlet amplitude
A_i = inlet amplitude
$A(0)$ = amplitude of inlet concentration waves
$A(z)$ = amplitude of concentration wave at z
$A_n(0)$ = amplitude of n-th harmonic in periodic wave
b = constant
b_n = coefficients of sine terms of Fourier series
B = function representative of the decrease in amplitude of outlet wave
c = concentration of tracer in solution, moles/unit volume or g./unit volume
c_m = mean composition about which concentration oscillates in frequency response experiments
c_n = concentration values employed in numerical harmonic analysis
c_0 = initial concentration of solution admitted to bed
C = constant
$-\frac{\partial c}{\partial y}$ = concentration gradient, moles/(cu. ft.)/(ft.)
d_p = particle diameter, in.
d_t = tube or column diameter, in. or ft.
D_L = effective axial diffusivity, sq. ft./sec.
D_R = effective radial diffusivity, sq. ft./sec.
D_T = total effective diffusivity, sq. ft./sec.
D_s = molecular diffusivity, sq. ft./sec.
k_n = adsorption velocity constant, sec.$^{-1}$
n = number of harmonic
N = mass transfer rate, moles/(sec.)(sq. ft.)
Pe = Peclet number; radial, $d_p u/D_R$ or axial, $d_p u/D_L$
Q = quantity of tracer injected in pulse function experiments, moles
r = radial coordinate in cylindrical coordinate system
R = dimensionless time ratio, ut/z
Re = Reynolds number, $d_p v_0 \rho/\mu$ or $d_p u\rho/\mu$
S = dimensionless diffusivity ratio, D_L/zu
t = time, sec.
u = mean linear velocity (interstitial velocity), ft./sec.
v_0 = superficial velocity based on empty column, ft./sec.
V = void volume of bed, cu. ft.
z = longitudinal coordinate in cylindrical coordinate system

Greek Letters

γ = function of adsorption velocity constant, equivalent to $1 + k_1/\epsilon$
δ = angle of periodic wave, equivalent to $(\omega t - \phi)$
δ_E = mixing diffusivity, sq. ft./sec.
ϵ = fraction void or porosity of packed bed
η = amount of tracer adsorbed on particle surface, moles/unit volume of bed
μ = viscosity of solution, centipoise
ρ = density of solution, g./cc.
ϕ = function representative of the phase shift of outlet wave
ψ = phase lag of n-th harmonic in periodic wave
ω = angular frequency of periodic wave, rad./sec.

LITERATURE CITED

1. Aris, R., and N. R. Amundson, *A.I.Ch.E. J.*, **3**, 280 (1957).
2. Baron, T., *Chem. Eng. Progr.*, **48**, 118 (1952).
3. Bernard, R. A., and R. H. Wilhelm, *Chem. Eng. Progr.*, **46**, 233 (1950).
4. Danckwerts, P. V., *Chem. Eng. Sci.*, **2**, 1 (1953).
5. Deisler, P. F., and R. H. Wilhelm, *Ind. Eng. Chem.*, **45**, 1219 (1953).
6. Ebach, E. A., Doctoral dissertation, Univ. Michigan, Ann Arbor, Michigan (June, 1957).
7. Fahien, R. W., and J. M. Smith, *A.I.Ch.E. J.*, 1, 28 (1955).
8. Hirai, E., *Chem. Eng.* (*Japan*), **18**, 528 (1954).
9. Klinkenberg, A. and F. Sjenitzer, *Chem. Eng. Sci.*, **5**, 258 (1956).
10. Kramers, H., and G. Alberda, *Chem. Eng. Sci.*, **2**, 173 (1953).
11. Lapidus, L., and N. R. Amundson, *J. Phys. Chem.*, **56**, 984 (1952).
12. Latinen, G. A., Ph.D. thesis, Princeton University (1951).
13. Levenspiel, O. and W. K. Smith, *Chem. Eng. Sci.*, **6**, 227 (1956).
14. McHenry, K. W., and R. H. Wilhelm, *A.I.Ch.E. J.*, **3**, 83 (1957).
15. Plautz, D. S., and H. F. Johnstone, *A.I.Ch.E. J.*, **1**, 193 (1955).
16. Rider, P. R., "Modern Statistical Methods," John Wiley & Sons, Inc., New York (1947).
17. Schwartz, C. E., and J. M. Smith, *Ind. Eng. Chem.*, **45**, 1209 (1953).
18. Thatcher, C. M., Ph.D. thesis, University of Michigan, Ann Arbor, Michigan (1954).
19. Wehner, J. F., and R. H. Wilhelm, *Chem. Eng. Sci.*, **6**, 89 (1956).
20. Wilhelm, R. H., *Chem. Eng. Progr.*, **49**, 150 (1953).
21. Wylie, C. R., "Advanced Engineering Mathematics," McGraw-Hill Book Company, Inc., New York (1951).
22. Yagi, S., and T. Miyauchi, *Chem. Eng.* (*Japan*), **19**, 507 (1955).

Manuscript received July 8, 1957; revision received Feb. 27, 1958; paper accepted March 13, 1958.